Tuijin Jishu/Journal of Propulsion Technology
ISSN: 1001-4055
Vol. 45 No. 1 (2024)

Numerical Analysis of Seismic Performance in High-Performance Fiber-Reinforced Cementitious Composite (HPFRCC) Frames

Meysam Ebrahimi Lakme Sari[1*], Fatemeh Nesa Mohajer Mojeni[2], Mohaddeseh Kalaei Moakhar[3]

1. PhD student, Civil Engineering - Construction Engineering and Management, Islamic Azad University, Neyshabur branch, Iran.
2. graduate, MSc, Civil-Structural Engineering, Yamili Institute of Higher Education, Gorgan, Iran
3. Master's student in architecture, Gorgan Institute of Higher Education, Iran

Abstract:- Considering the importance of moment frames in concrete structures, reinforcing them with high performance fibers is very effective. High-performance fiber reinforced cementitious composite (HPFRCC) materials exhibit strain hardening behavior under tension and can be used in seismic rehabilitation of structural members. The aim of this research is to evaluate the seismic performance of reinforced concrete and compare them with reinforced concrete frames, which was carried out using the numerical analysis method and ABAQUS finite element software to model a moment frame under different loads. After validating the software performance, the modeling of the conventional reinforced concrete frame was conducted. Then, its panel zone was replaced by HPFRCC materials with different resistances and different percentages of reinforcements, and it was compared with reinforced concrete frame and reinforced HPFRCC frame. The results showed that with the increase of the vertical force on the frame, the yield corresponding lateral displacement in reinforced concrete, reinforced composite HPFRCC and HPFRCC frames decreased 13-41%, 24-41% and 17-34%, respectively. Lateral bearing capacity in reinforced concrete, reinforced composite HPFRCC and HPFRCC frames decreased 1-2%, 1-4% and 2-7%, respectively. In HPFRCC frames, by increasing the size of rebars from 12 to 14 mm and 16 mm, the force increased by 5% and 20%, respectively, and the lateral displacement decreased by 3% and 4.5%, respectively. By increasing the reinforcement area in the frame columns of all frames, the plastic hinge length (l_P) and the plastic hinge rotation (θ_P) decreased in the columns and increased in the beam.

Keywords*: HPFRCC frame, Finite element method, Seismic, Bearing capacity, Plastic hinge*

1. Introduction

Fiber reinforced cementitious composites (FRCC) have made many impressive advances in recent years, due to the further development of mortar, different types of fibers, mortar-fiber interaction, composite production process, better understanding of the main mechanisms, behavior control and continuous improvement of operational costs. It is also possible to mention the introduction of a new generation of additives (super-lubricants) in order to achieve high resistances with the least reduction in mortar efficiency, the use of fine fillers such as silica fume and fly ash and also a better understanding of how they affect the porosity, resistance and durability of the mortar. All of the mentioned cases have caused fundamental developments in the construction and modeling of the behavior of these composites. Using high performance materials instead of conventional materials, in addition to increasing the capacity of structures against earthquakes, they also help to provide more reliability of structures against harmful environmental factors. One of these high-performance materials, which has made significant progress in recent years, is high performance fiber reinforced cementitious composites (HPFRCC). The strain hardening behavior under tension of HPFRCC, which is different from other cementitious and concrete composites, has made it a high performance material with high

energy absorption and high cracking capabilities before failure. In recent years, the use of HPRFCC materials to build earthquake-proof structures has received attention. One of the features that makes the HPFRCC suitable for performing restoration operations and replacing conventional concrete is the possibility of creating a strong bond between it and the concrete due to their structural similarity. Abushawashi and Vimonsatit [1] conducted a laboratory study on the use of ferrocement panels as reinforced concrete slabs with lightweight blocks infill. They experimented ferrocement control panels and hybrid ferrocement panels to investigate the strength capacity and hard strain behavior through flexure, toughness and multitrack forming. The results showed that by using the ideal fiber/wire mesh content, the hybrid ferrocement panels act as a strain-hardening cementitious material, and successfully increasing the flexure strength compared to the control-group ferrocement. Also, the hybrid PVA fiber ferrocement in tensile zones can be successfully used as permanent form.Jiri and Petr [2] studied the field tests of concrete slabs made from the HPFRC. They conducted explosions at the Boletice and Březina military training areas. The tests were divided into two types of PlNp 10 contact explosions, which investigated charge penetration through slabs, and distant explosions, which studied some other characteristics of the test cases. The main advantage of HPFRC is very high compressive strength, which allows to reduce the cross-section area and the weight of the whole building. Their results showed that HPFRC concrete slabs have a very good resistance against explosion charge. Ozyildirim et al. [3] investigated HPFRC structure that was a mixture of mortar with synthetic fibers and steel. The HPFRCC has high ductility and durability and can exhibit strain hardening leading to multiple cracks at large deformations. The mixture with synthetic fibers showed strain hardening with multiple microcracks. The results showed that the use of HPRFCC in continuous slabs and thin coating is possible.Yao et al. [4] studied HRBF500 grain reinforcement and C100 high-performance fiber reinforced cementitious composites in the civil air defense work. Their results showed that in a beam with same width and reinforcement, new materials can effectively reduce the height of the beam and a combination of two new materials has long-term importance in civil air defense work. In the same load, the HRBF500 grain reinforcing bar and C100 HPFRCC can be better matched in air defense work. They can reduce member sections and increase clearance with the same amount of material, the improvement of material properties can bring increased capacity. Adhikari and Patnaik [5] investigated the potential applications of steel fiber reinforced concrete in improving the seismic behavior of frame structures. They found that steel fiber reinforced concrete is a suitable ductile high performance material that is gaining acceptance for applications in frame structures and is particularly suitable for enhancing seismic response.Billington et al. [6] studied response of high performance fiber reinforced concrete infill panels retrofitting steel moment-resisting frames. They found that the SC-HPFRC panels performed similarly in the component and hybrid simulation experiments with the exception of the degree of multiple cracking. In both cases the primary mode of panel failure was flexural and the SC-HPFRC was robust against spalling and bearing loads. Damage of the infill panels in the hybrid experiment was well distributed as designed. Dehghani et al. [7] designed the cementitious composites for strengthening masonry-infilled reinforced concrete frames. Thay stated that the suggested ECC-strengthening method can effectively increase the lateral strength and energy absorption capacity of the infilled frame, prevent brittle failure modes in the infill wall, and provide a reasonable system overstrength. Fukuyama et al. [8] investigated the HPFRCC device for seismic response control. Their results showed that HPFRCC devices are able to significantly reduce response deformation of the steel frame. The use of HPFRCCs instead of concrete can lead to better control of failure mechanism, deformation capacity, hysteresis characteristics and damage rate of reinforced concrete members.Hemmati et al. [9] studied the ductile behavior of HPFRCC frames. They developed 3D nonlinear numerical model using the finite element (FE) method. The results indicated that using HPFRCC materials, instead of normal concrete in reinforced concrete frames, increased the ultimate load, ultimate deflection, ductility ratio, and plastic hinge characteristics of frames. Also, they found that the addition of fibers in concrete frames increased the energy absorption and increasing the amount of the vertical load changed the development of plastic hinges in analytical frames. Maya and Albajar [10] studied beam-column connections for precast concrete frames using HPFRCCs. The main connection mechanism was the connection of the longitudinal beam reinforcement, which was occurred at the end of the beam elements, outside the connection area. The proposed configuration avoided interference between longitudinal and transverse reinforcements, reduced in situ work and allowed defining an efficient and safe construction process.According

to the conducted studies, most of the research have been focused on knowing the nature of these materials, their different compositions, different mixing ratios of materials, relationships governing the stress-strain curve, inventing new composites and other similar cases. Although some research has also been conducted on its practical applications in structures, these studies are not as extensive as the research related to knowing the behavior of the materials, and it requires much analytical and laboratory work based on the relationships that govern the conduct of materials. Therefore, it seems necessary to perform more studies on the structural and practical issues of high performance materials, and the seismic behavior of beams and frames made with these materials. The purpose of this study is to investigate the behavioral patterns of the structure, focusing on the seismic behavior of frames made with HPFRCC materials. Therefore, the force curves against the displacement of these structures were drawn to compare the ductility of these composite frame with reinforced concrete and reinforced HPFRCC frames. Also, the formation, location and characteristics of plastic hinges in these frames were also compared. Therefore, the seismic behavior of these structures was studied by performing finite element numerical studies using ABAQUS software on the frames under constant vertical and lateral loading in order to determine the effect of using ductile concrete in reinforced concrete structures.

2. Materials and methods

2.1 Model specifications

In this research, three 3D reinforced concrete moment frames with a bay of 3 m and a height of 20.3 m were modeled by ABAQUS v6.14 finite element software. The beam section and the column section were 0.15*0.2 m^2 and 0.2*0.2 m^2, respectively. The materials used in the first model were normal concrete (RC) and in the second and third models were HPFRCC in reinforced form (RH) and reinforced composite HPFRCC (RCH) as shown in Fig. 1.

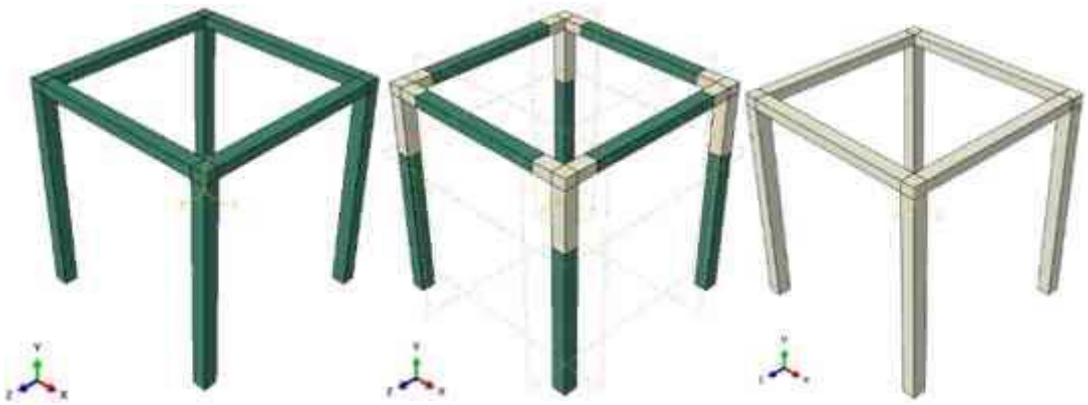

Figure 1: The models made by Abaqus software (RCH-RH and RC models).

2-2- Material specifications

Table 1 presents the specifications of the materials used to make the models in the software, including normal concrete, HPFRCC, and steel.

Table 1: Specification of different material.

Characteristic	Concrete	HPFRCC	Steel
f'_c (MPa)	25	25	
f_y (MPa)			400
E (MPa)	25,000	30,000	210,000
Density (kg/m^3)	2,400	2,400	7,850
Poisson's coefficient	0.18	0.2	0.3

2-3- Concrete modelling

According to the axial stress-strain curve of concrete, this material has a linear behavior to a certain extent, and after that the behavior of concrete is completely non-linear. In case of full unloading in the non-linear region,

the strain in the concrete is not zero and the sample is permanently deformed. To introduce the linear behavior of concrete, Poisson's coefficient and elastic modulus are required. Poisson's coefficient of concrete is in the range of 0.15 to 0.20 and the elastic modulus is obtained from Eq. 1.

$$E = 4700\sqrt{f_c'} \quad (1)$$

where, f_c' (MPa) is the strength of concrete.

Damaged plasticity model or Drucker-Prager model can be used to define the plastic behavior of concrete. The Drucker-Prager model and the damaged plasticity model use the concepts of plasticity and the combination of plasticity and damage to express the nonlinear behavior of concrete, respectively. There are two other models in the Abaqus software: Concrete smeared cracking and cracking model for concrete. The first model is used for cases where cracking controls the behavior of concrete, and the second model considers the behavior of concrete under pressure to be linear and is used for cases where concrete is under tensile loading. In this research, damaged plasticity model was used to model the behavior of concrete enclosed with FRP. The damaged plasticity model includes three components: flow potential rule, yield criterion, and hardening rule.

Considering the necessity of 3D modeling and in order to allocate the element that provides the behavior of concrete in this case, it is possible to use 3D solid eight-node elements (C3D8R). The suffix R is used to reduce the integration points in order to decrease the duration of the program execution. One of the reasons for choosing this type of element is to have less convergence problem and higher accuracy of solutions. One of the drawbacks of this type of element is the very hard meshing of the models. In general, solid element points can be bound for three degrees of freedom which include (u_x, u_y, u_z) and as a result, appropriate support conditions can be applied on the samples.

2-4- Reinforcement modelling

The elastic modulus of and Poisson's coefficient of steel were equal to 2.1×10^5 and 0.3 MPa, respectively, which indicates its elastic behavior. The behavior after yielding was defined by inelastic stress-strain as a tabular function for the software. The inelastic strain is equal to the difference between the total strain and the elastic strain. The relationship between total, inelastic and elastic strains is as follows:

$$\varepsilon_{el} = \frac{\sigma}{E_s} \quad (2)$$

$$\varepsilon_{in} = \varepsilon_t - \varepsilon_{el} \quad (3)$$

where ε_{el}, ε_{in}, and ε_t are elastic, inelastic and total strains, respectively. σ and E_s are axial stress and elastic modulus of steel, respectively.

Rebars can be modeled using 3D element or 2D truss element, but there is not much difference in the results of these two methods. 2D truss element was used to model steel rebars in this study. This two-node element has the ability to model the nonlinear behavior of steel. To model the relationship between rebars and concrete as well as the unit performance of this material, a constraint called Embedded was used. This constraint embeds the reinforcement inside the concrete and calculates the freedom degrees of the rebars from the interpolation of the freedom degrees of the surrounding concrete.

2-5- Determining earthquake records for ABAQUS software input

Information related to earthquakes and accelerogram were obtained through the PEER global site. For this purpose, information on acceleration (ATH), velocity (VTH) and displacement (DTH) was obtained for the earthquake in three vertical, x and y directions. After receiving the earthquake data, in order to match the information and enter them into the ABAQUS software, the data was levelled by the Seismosignal software. In this study, the information of Tabas (Yazd) earthquake in 1978 with maximum acceleration of 0.85 g, Landers California earthquake in 1992 with a maximum acceleration of 0.789 g and Kobe (Japan) earthquake in 1995 with a maximum acceleration of 0.671 g were used. According to the analyzes performed for the three mentioned earthquakes, their accelerograms are shown in Figs. 2-4.

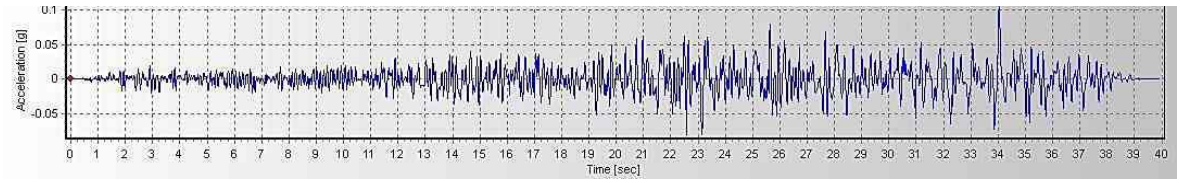

Figure 2: Accelerogram of Tabas earthquake with Richter scale 7.8.

Figure 3: Accelerogram of Landers earthquake with Richter scale 7.3.

Figure 4: Accelerogram of Kobe (Japan) earthquake with Richter scale 7.3.

Results and discussion

3-1- Lateral force-lateral displacement curve and formation process of plastic hinges

3-1-1- Reinforced concrete frame (RC)

Due to the application of a vertical force of 10 kN calculated based on the virtual load combination model (live load of 200 kg/m^2 and dead load of 560 kg/m^2 is considered), the first plastic hinge was created at the upper edge of the link beams and the connection point with the column on the opposite side of the force. With the increase of the lateral load, the next hinges were created at the inner edge of the fondation connection to the column on the opposite side of the force. By changing the vertical loading in order to evaluate the structure under heavier loads, vertical forces of 20 and 30 kN were applied to the surface of the beams to show the formation process of plastic hinges in the concrete frame. With the application of these forces, the first plastic hinge was formed at the upper edge of the link beams and at the connection point with the column on the opposite side of the force. With the increase in lateral load in these two cases, the next plastic hinges were also formed in the panel zone on the opposite side of the force and the inner edge of the connection of the column on the opposite side of the force.

Creating plastic hinges in the analytical model can be considered similar to creating cracks in the real model. Indeed, the position of the plastic hinges created in the software model are the areas prone to cracking in the structure, which must be reinforced. Fig. 5 shows the location of the plastic hinges in the reinforced concrete frame (RC) at the failure moment.

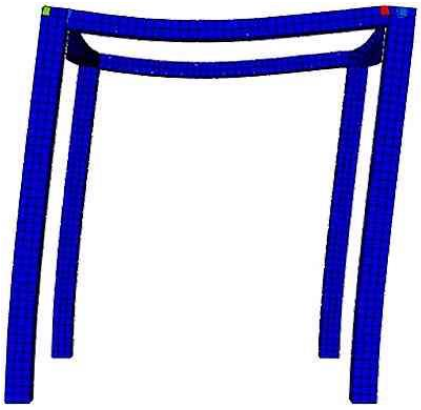

Figure 5: The position of the plastic hinge in the reinforced concrete frame (RC).

Figs. 6 and 7 show the formation process of plastic hinges in the reinforced concrete frame under the influence of different vertical loadings.

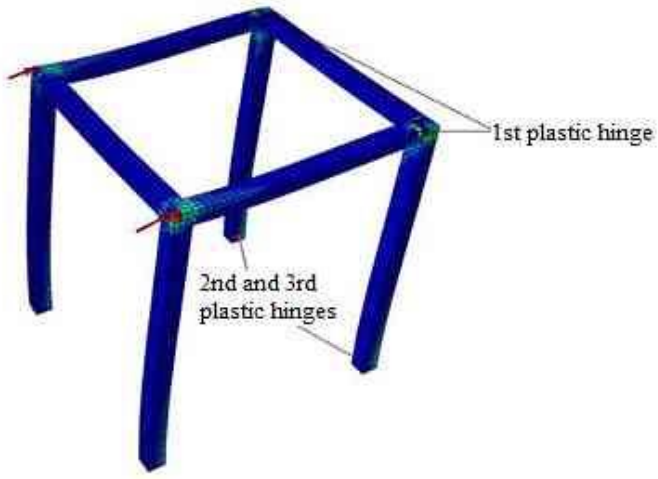

Figure 6: The order of plastic hinge formation in the reinforced concrete frame (RC) with a vertical force of 10 kN.

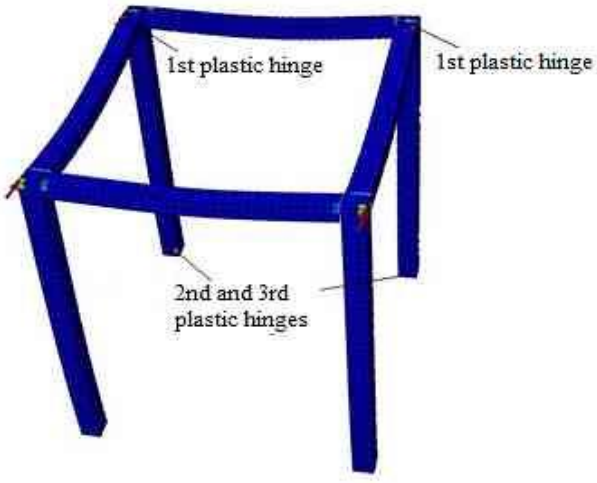

Figure 7: The order of forming plastic hinges in the reinforced concrete frame (RC) with vertical force of 20 and 30 kN.

The lateral force-lateral displacement curve of the RC frame is shown in Fig. 8.

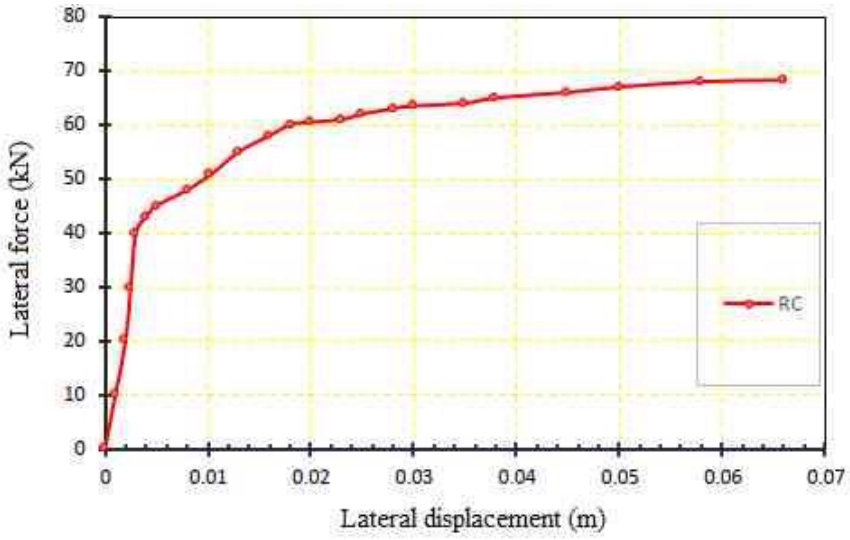

Figure 8: The lateral force-lateral displacement curve of the analytical model of the RC frame with f'_c=25 MPa.

Fig. 9 also shows the lateral force-lateral displacement curves of reinforced concrete frames with different vertical forces.

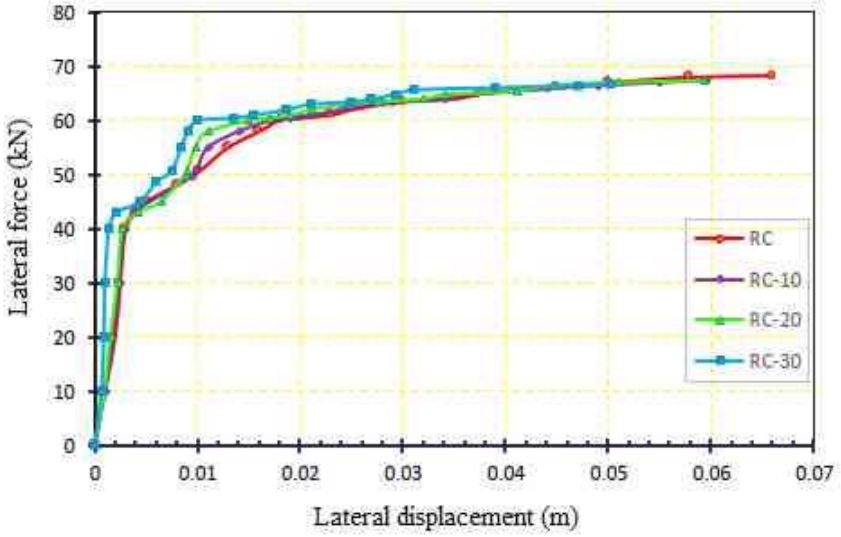

Figure 9: The lateral force-lateral displacement curve of the RC frame with different vertical forces.

A summary of the analytical results of different reinforced concrete frames (RC) is provided in Table 2.

Table 2: Analytical results of reinforced concrete frames with different vertical forces.

Model	P_y (kN)	Δ_y (mm)	P_u (kN)	Δ_u (mm)	$\mu = \frac{\Delta_u}{\Delta_y}$	$\frac{P_u}{P_{u\,RC}}$	$\frac{\mu_u}{\mu_{u\,RC}}$
RC	50.70	10.22	68.28	66.00	6.46	1	1
RC-10	49.83	9.49	67.47	59.54	6.27	0.988	0.971
RC-20	49.93	8.85	67.41	59.28	6.69	0.987	1.036
RC-30	48.70	6.04	66.81	50.19	8.31	0.978	1.29

According to the data in Table 2, it seems that the yield force in the frame remained almost constant with the increase in the vertical force on the frame. But the yield corresponding lateral displacement decreases about 13-41%. This can be caused by the increase in the tension of the reinforcements due to the application of more vertical load, which causes them to yield in less lateral displacement. The lateral bearing capacity of the frame also decreased by 1-2%. This can be caused by applying a vertical load and preventing premature tensile cracks in the columns, which causes the failure mechanism to be changed and the first hinge to be transferred from the column to the beam and the capacity of the beam to be used more. Meanwhile, the ductility also increases by 3-59% compared to the RC frame.

3-1-2- Reinforced composite HPFRCC frame (RCH)

Due to the application of a vertical force of 10 kN, the first plastic hinge was created in the panel zone of the opposite side of the force and the inner edge of the foundation connection to the column on the opposite side of the force, but its amount was much less than the damage that can be seen in the RC frame (Fig. 5). With the increase in the lateral load, the next hinges were created in the same place as before. By changing the vertical loading and applying a vertical force of 20 kN to the RCH frame, the first plastic hinge is formed in the beam on the opposite side of the force. With the increase in the seismic load, the next plastic hinges are formed in opposite columns. On the other hand, by applying a vertical force of 30 kN to the frame, the first plastic hinge was formed in the panel zone of opposite side the force and the outer edge of the foundation connection point of the left column. With the increase in the seismic load, the next plastic hinges are formed in the same place as before. Fig. 10 shows the position of the plastic hinges in the reinforced composite HPFRCC frame (RCH) at the failure moment.

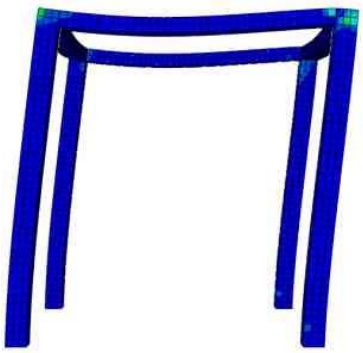

Figure 10: The position of the plastic hinge in the reinforced composite HPFRCC frame (RCH).

Figs. 11 and 12 show the formation process of plastic hinges in the reinforced composite HPFRCC frame under different vertical loadings.

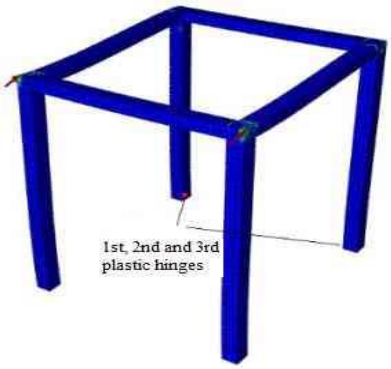

Figure 11: The order of plastic hinge formation in the reinforced composite HPFRCC frame (RCH) with a vertical force of 10 kN.

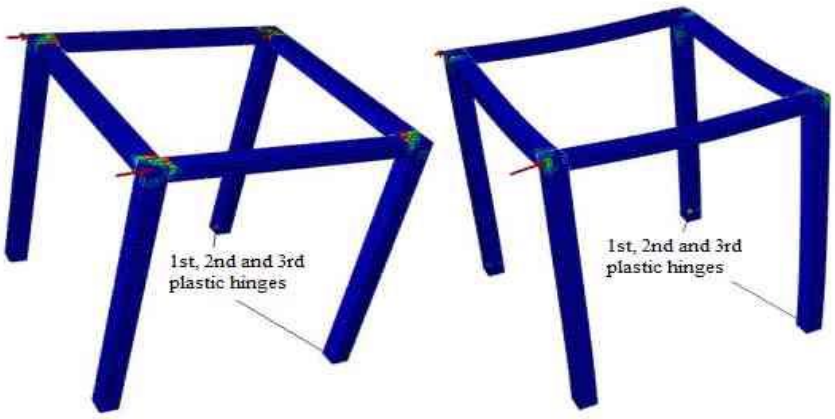

Figure 12: The order of plastic hinge formation in the reinforced composite HPFRCC frame (RCH) with vertical forces of 20 and 30 kN.

The lateral force-lateral displacement curve of the RCH frame is shown in Fig. 12.

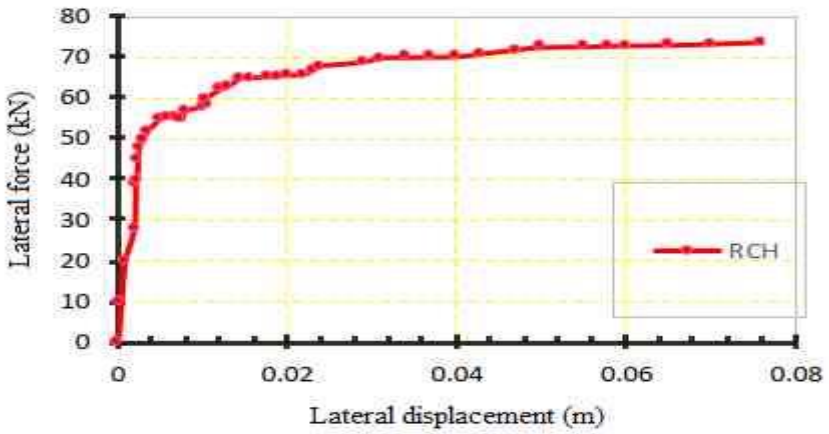

Figure 13: The lateral force-lateral displacement curve of the analytical model of the RCH frame.

Fig. 14 also shows the lateral force-lateral displacement curves of RCH frame with different vertical forces.

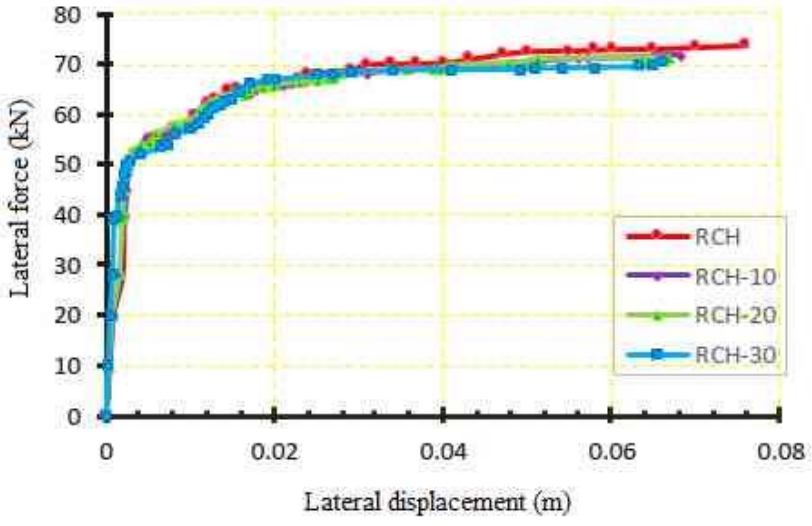

Figure 14: The lateral force-lateral displacement curve of the RCH frame with different vertical forces.

A summary of the analytical results of different reinforced composite HPFRCC frames (RCH) is given in Table 3.

Table 3: Analytical results of RCH frames with different vertical forces.

Model	P_y (kN)	Δ_y (mm)	P_u (kN)	Δ_u (mm)	$\mu = \frac{\Delta_u}{\Delta_y}$	$\frac{P_u}{P_{u\,RC}}$	$\frac{\mu_u}{\mu_{u\,RC}}$
RC	50.70	10.22	68.28	66.00	6.46	1	1
RCH	58.57	10.59	73.81	76.00	7.18	1.08	1.11
RCH-10	57.41	10.03	71.72	68.26	6.81	1.05	1.05
RCH-20	57.79	8.03	71.26	66.74	8.31	1.04	1.29
RCH-30	53.64	6.56	70.63	66.07	10.07	1.03	1.56

The results show that with an increase in the vertical force on RCH frames, the yield corresponding lateral displacement decreased by 24-41%. It can be caused by the increase in the tension of the reinforcements due to the application of more vertical load, which causes them to yield in less lateral displacement. The lateral bearing capacity of the frame also decreased by 1-4%. This can be caused by applying a vertical load and preventing premature tensile cracks in the columns, which causes the failure mechanism to be changed and the first hinge to be transferred from the column to the beam and the capacity of the beam to be used more. Furthermore, the ductility and tolerable lateral force also increases by 5-77% and 3-17%, respectively compared to the RC frame.

3-1-3- Reinforced HPFRCC frame (RH)

Due to the application of a vertical force of 10 kN, the first plastic hinge was created at the connection point of the beam to the column on the side of the force, but its amount was much less than the damage that can be seen in the RC and RCH frames (Fig. 15).

Figure 15: The position of the plastic hinge in the reinforced HPFRCC frame (RH).

With the increase in the lateral load, the next hinges were created in the panel zone of the opposite side of the force and the inner edge of the foundation connection to the right column. By applying the vertical forces of 20 and 30 kN to the frame, the first plastic hinge was formed at the upper edge of left beam at the connection point with the column. With the increase in the seismic load, the next plastic hinges are formed in the left beam and in the inner edge. Figs. 16 and 17 show these results.

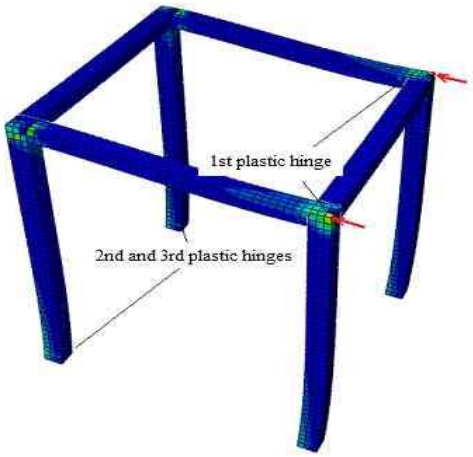

Figure 16: The order of plastic hinge formation in the reinforced HPFRCC frame (RH) with a vertical force of 10 kN.

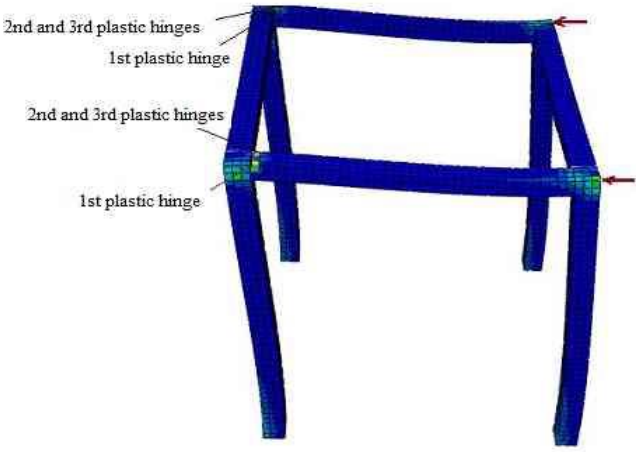

Figure 17: The order of plastic hinge formation in the reinforced HPFRCC frame (RH) with vertical forces of 20 and 30 kN.

Fig. 18 shows the lateral force-lateral displacement curve of the RH frame and Fig. 19 also shows the lateral force-lateral displacement curve of RH frames with different vertical forces.

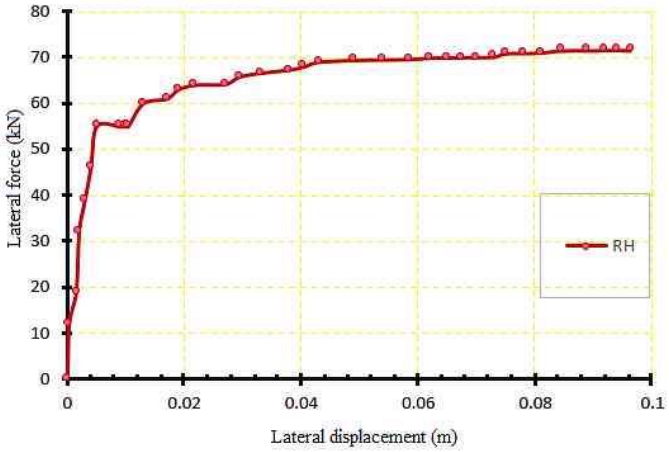

Figure 18: The lateral force-lateral displacement curve of the analytical model of the RH frame.

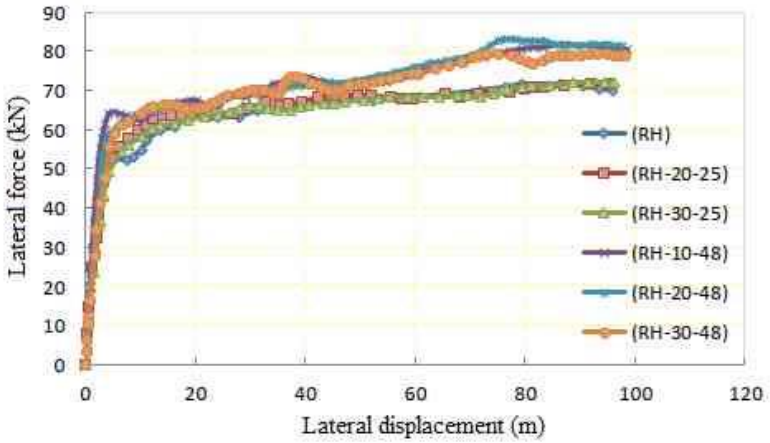

Figure 19: The lateral force-lateral displacement curve of the RH frame with different vertical and compressive strength.

Table 4 shows a summary of the analytical results of reinforced HPFRCC frames (RH).

Table 4: Analytical results of RH frames with different vertical forces.

Model	P_y (kN)	Δ_y (mm)	P_u (kN)	Δ_u (mm)	$\mu = \frac{\Delta_u}{\Delta_y}$	$\frac{P_u}{P_{u\,RC}}$	$\frac{\mu_u}{\mu_{u\,RC}}$
RC	50.70	10.22	68.28	66.00	6.46	1	1
RH	54.96	10.04	71.47	96.36	9.59	1.05	1.48
RH-20	57.48	8.29	71.78	95.50	11.52	1.05	1.78
RH-30	54.45	6.63	72.75	96.03	14.48	1.07	2.24

It seems that with the increase in the vertical force on the reinforced HPFRCC frames, the yield corresponding lateral displacement decreased by 17-34%. It can be caused by the increase in the tension of the reinforcements due to the application of more vertical load, which causes them to yield in less lateral displacement. The lateral bearing capacity of the frame also decreased by 2-7%. This can be caused by applying a vertical load and preventing premature tensile cracks in the columns, which causes the failure mechanism to be changed and the first hinge to be transferred from the column to the beam and the capacity of the beam to be used more. Furthermore, the ductility and tolerable lateral force also increases by 1.48-2.25 times and 5-20%, respectively compared to the RC frame.

3-2- Comparison between RC, RCH, and RH frames

The lateral force-lateral displacement curve of RC-10, RCH-10 and RH-10 frames is shown in Fig. 20.

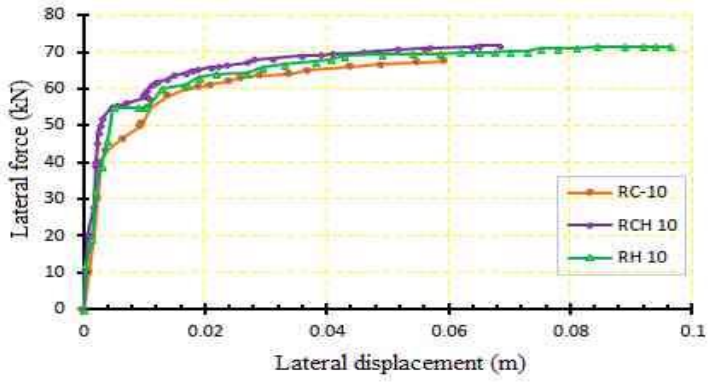

Figure 20: Lateral force-lateral displacement curves of reinforced concrete, reinforced composite HPFRCC and reinforced HPFRCC frames with the same vertical force.

It can be seen that under the same conditions (vertical load of 10 kN and compressive strength of 48 MPa), the lateral force and lateral displacement of the RH frame increased by about 3.3% and 25.8%, respectively, compared to the RCH frame. Also, the lateral force and lateral displacement of the RH frame increased by about 20.3% and 49.8%, respectively, compared to the RC frame.

3-2-1- Plastic hinges

The conditions that a reinforced concrete beam is subjected to in the final state under a uniform extensive load are shown in Fig. 21. In the case of moments that are smaller than the yield moment of the beam (M_y), the curvature of the beam increases gradually from the free edge of the beam (A) towards the support (B). This increases suddenly and further after the yield moment, and as a result, it reaches the maximum curvature value at the edge of the support. According to Fig. 21, the curvature distribution over the beam length can be divided into elastic and plastic. Therefore, the total beam rotation (θ_{total}) can be divided into elastic (θ_e) and plastic (θ_P).

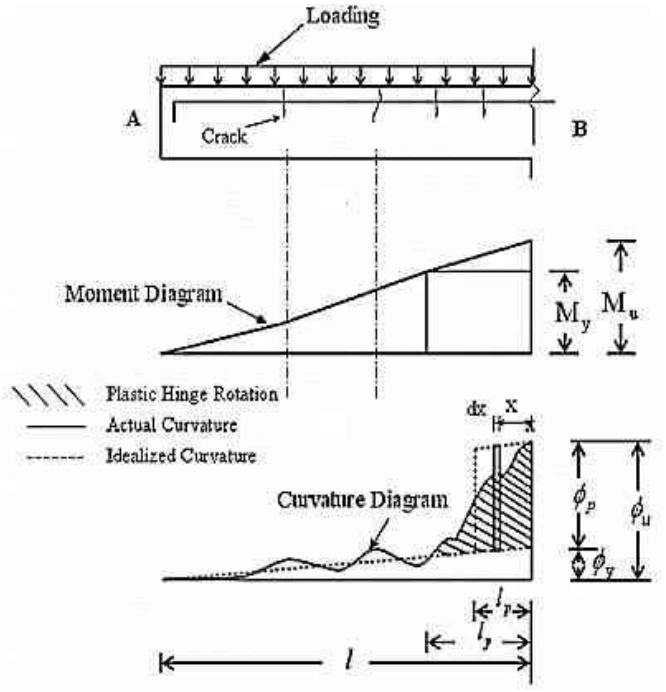

Figure 21: Distribution of curvature along the beam length in the final state.

The section plastic rotation can be obtained through Eq. 4.

$$\theta_p = \int_0^{l_y} [\phi(x) - \phi_y]\, dx \tag{4}$$

where l_y is yield length. It is the length of the beam in which the moment in the beam is greater than the yield moment. $\phi(x)$ and ϕ_y also show the curvature of each section of the beam and the yield curvature, respectively.

The section plastic rotation is equal to the hatched area of Fig. 21. If this hatched area is equated to a rectangle, the length of this rectangle (l_p) is obtained from the Eq. 5:

$$l_p = \frac{1}{\phi_u - \phi_y} \int_0^{l_y} [\phi(x) - \phi_y]\, dx \tag{5}$$

where ϕ_u is ultimate curvature.

Therefore, the relationship between θ_P and l_P is calculated using Eq. 6:

$$\theta_p = (\phi_u - \phi_y) l_p = \phi_p l_p \tag{6}$$

The curvature distribution in the columns on the force side and opposite side of the force is shown in Figs. 22 and 23. As can be seen in these figures, the yield length of reinforcement and curvature value in RH frames is more than RCH frames. On the other hand, these parameters in RCH frames are more than RC frames.

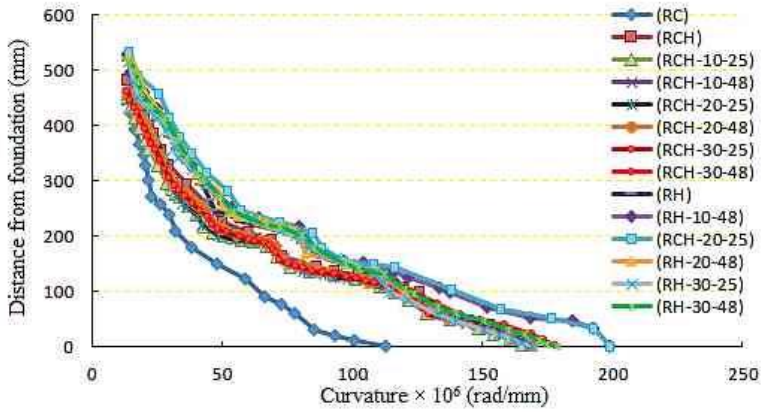

Figure 22: Curvature distribution in the column related to the force side.

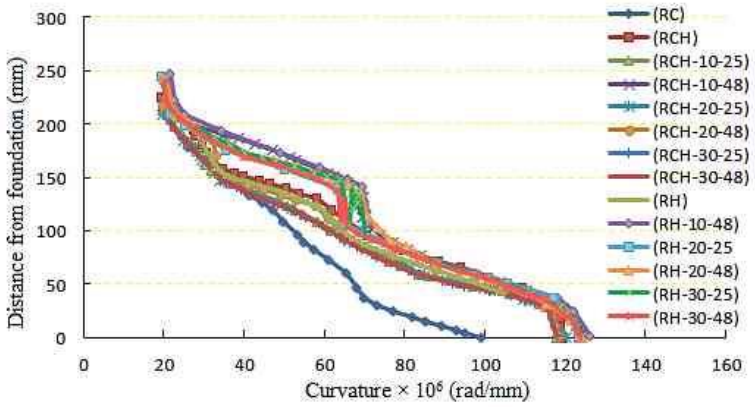

Figure 23: Curvature distribution in the column related to the opposite side of the force

A summary of the analytical results is presented in Table 5. Based on the obtained results, by increasing the compressive strength of concrete or HPFRCC, the amount of curvature and length of the plastic hinge increases. An increase in the vertical force caused a change in the failure mode, curvature and length of the plastic hinge in the columns, while it results in an increase in these parameters in the beams. Furthermore, the curvature value and the length of the plastic hinge in the studied RH frame increases by about 22-30% and 2.06 to 2.43 times, respectively compared to the RC frame. The increase in the case of the RCH frame were about 6-18% and 64-87%, respectively compared to the RC frame.

Table 5: A summary of the analytical results related to the plastic hinge of the frames.

Model	Formation place	l_y (mm)	$\theta_p \times 10^6$ (rad)	l_p (mm)
RC	The column on the opposite side of the force	210	0.0087	110
	The beam on the opposite side of the force	245	0.0101	128
	The column on the force side	420	0.0157	159
RCH	The column on the opposite side of the force	224	0.0126	127
	The beam on the opposite side of the force	259	0.0146	146
	The column on the force side	480	0.0295	188

Model	Formation place	l_y (mm)	$\theta_p \times 10^6$ (rad)	l_p (mm)
	The column on the opposite side of the force	210	0.0112	115
RCH-10	The beam on the opposite side of the force	280	0.0150	153
	The column on the force side	450	0.0267	175
	The column on the opposite side of the force	442	0.0263	172
RCH-20	The beam on the opposite side of the force	245	0.0131	134
	The column on the force side	206	0.0111	113
	The column on the opposite side of the force	435	0.0258	169
RCH-30	The beam on the opposite side of the force	280	0.0150	153
	The middle of the beam span	238	0.0127	130
	The column on the opposite side of the force	245	0.0142	137
RH	The beam on the opposite side of the force	280	0.0163	157
	The column on the force side	525	0.0374	205
	The column on the opposite side of the force	525	0.0324	203
RH-20	The beam on the opposite side of the force	294	0.0164	157
	The middle of the beam span	287	0.0160	153
	The column on the opposite side of the force	476	0.0338	194
RH-30	The beam on the opposite side of the force	294	0.0164	157
	The middle of the beam span	287	0.0160	153

3-2-2- Effect of column reinforcements

In order to investigate the influence of column reinforcements on the process and order of plastic hinge formation, other models with different reinforcements were analyzed. The column reinforcements of the original models were 12 mm in diameter. But in the new models, 14 and 16 mm-diameter reinforcements were used. The naming of new models was based on the same basis as the previous models, with the difference that a number is mentioned at the end as the reinforcement diameter. As an example, the RCH-10-48-16 model is a reinforced composite HPFRCC model in which the vertical load is 10 kN, the compressive strength is 48 MPa, and the diameter of the column reinforcement is 16 mm. It should be noted that the wire element is used to model the reinforcement in ABAQUS software, which can be modeled the reinforcement with different diameters by changing its specifications. Figs. 24-26 show the lateral force-lateral displacement curve of reinforced concrete (RC), reinforced composite HPFRCC frame (RCH) and reinforced HPFRCC (RH) models with different reinforcements, respectively.

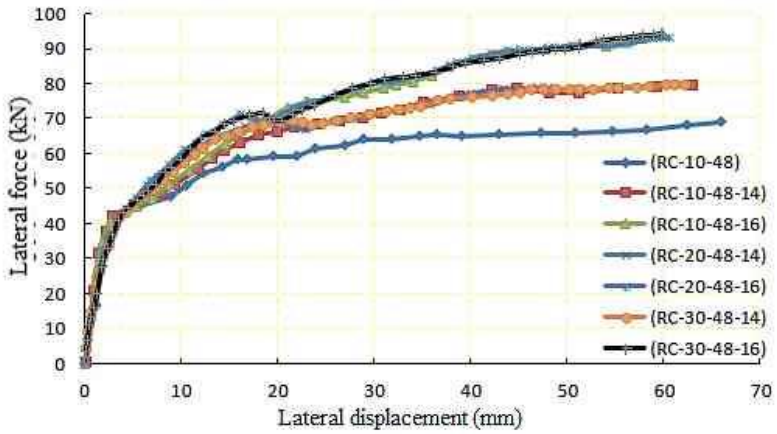

Figure 24: Lateral Force-Lateral displacement curves of reinforced concrete frames with different reinforcements.

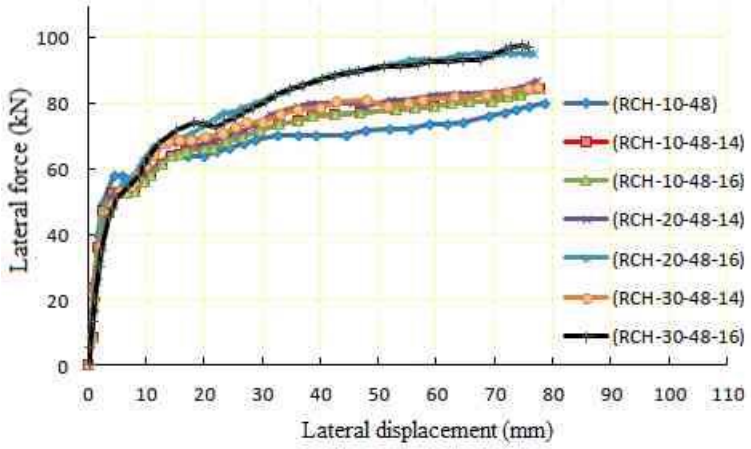

Figure 25: Lateral Force-lateral displacement curves of reinforced composite HPFRCC frames with different reinforcements.

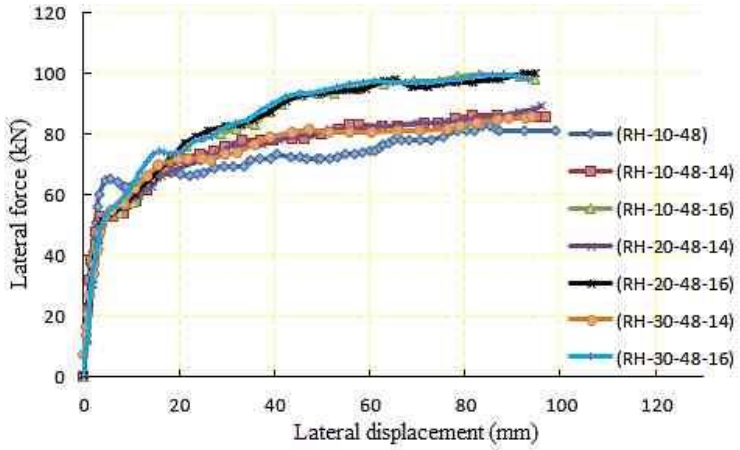

Figure 26: Lateral Force-lateral displacement curves of reinforced HPFRCC frames with different reinforcements.

As can be seen in these figures, with the increase in the area of the reinforcements in the columns, the final force of the frames increases, but their final displacement does not change much. In reinforced concrete frames with columns with 14 mm and 16 mm diameter reinforcements compared to the frame with columns with 12 mm diameter reinforcements, the force increased by about 16% and 36%, respectively, while the lateral displacement decreased by about 5.5% and 8%, respectively.

In the reinforced composite HPFRCC frames with columns with 14 mm and 16 mm diameter reinforcements compared to the frame with columns with 12 mm diameter reinforcements, the force increased by about 7% and 21%, respectively, while the lateral displacement decreased by about 1.5% and 3%, respectively. Also, in reinforced HPFRCC frames with columns with 14 mm and 16 mm diameter reinforcements compared to the frame with columns with 12 mm diameter reinforcements, the force increased by about 5% and 20%, respectively, while the lateral displacement decreased by about 3% and 4.5%, respectively. Table 6 provides a summary of the analytical results that include lateral forces and maximum lateral displacement along with the characteristics of plastic hinges and their formation order.

Table 6: A summary of the analytical results of the frames with different reinforcements in the column.

Model	P_u (kN)	Δ_u (mm)	Hinge formation place	l_y (mm)	$\theta_p \times 10^6$ (rad)	l_p (mm)
RC-10-48	68.28	66.00	The beam on the opposite side of the force	245	0.0101	128
			The column on the opposite side of the force	210	0.0087	110
			The column on the force side	420	0.0157	159
RC-10-48-14	79.50	62.98	The beam on the opposite side of the force	247	0.0102	129
			The column on the opposite side of the force	196	0.0081	102
			The column on the force side	392	0.0147	149
RC-10-48-16	93.68	60.05	The beam on the opposite side of the force	250	0.0103	130
			The column on the opposite side of the force	175	0.0073	91.4
			The column on the force side	350	0.0131	133
RC-20-48-14	79.67	61.99	The beam on the opposite side of the force	259	0.0107	135
			The column on the opposite side of the force	189	0.0078	98.7
			The column on the force side	378	0.0141	143
RC-20-48-16	92.68	60.57	The beam on the opposite side of the force	266	0.0110	139
			The column on the opposite side of the force	161	0.0067	84.1
			The column on the force side	322	0.0120	122
RC-30-48-14	79.37	61.97	The beam on the opposite side of the force	273	0.0113	143
			The column on the opposite side of the force	168	0.0070	87.8
			The column on the force side	336	0.0126	128
RC-30-48-16	94.22	59.80	The beam on the opposite side of the force	287	0.0119	150
			The column on the opposite side of the force	147	0.0060	76.8
			The column on the force side	294	0.0110	112
RCH-10-48	79.57	78.62	The beam on the opposite side of the force	252	0.0139	141
			The column on the opposite side of the force	217	0.0120	121
			The column on the force side	465	0.0283	181
RCH-10-48-14	83.88	77.87	The beam on the opposite side of the force	266	0.0147	149
			The column on the opposite side of the force	196	0.0108	110
			The column on the force side	420	0.0256	164
RCH-10-48-16	96.83	76.94	The beam on the opposite side of the force	280	0.0154	156
			The column on the opposite side of the force	182	0.0103	103
			The column on the force side	390	0.0240	153
RCH-20-48-14	85.99	77.57	The beam on the opposite side of the force	285	0.0158	158
			The column on the opposite side of the force	203	0.0112	113
			The middle of the beam span	245	0.0135	137
RCH-20-48-16	95.36	76.65	The beam on the opposite side of the force	292	0.0173	161
			The column on the opposite side of the force	189	0.0106	104
			The middle of the beam span	247	0.0136	138
RCH-30-48-14	84.84	77.34	The beam on the opposite side of the force	302	0.0180	165
			The column on the opposite side of the force	182	0.0100	102
			The middle of the beam span	249	0.0137	139
RCH-30-48-16	96.76	75.85	The beam on the opposite side of the force	310	0.0185	167
			The column on the opposite side of the force	168	0.0093	93.9

Model	P_u (kN)	Δ_u (mm)	Hinge formation place	l_y (mm)	$\theta_p \times 10^6$ (rad)	l_p (mm)
			The middle of the beam span	251	0.0138	140
			The beam on the opposite side of the force	287	0.0169	161
RH-10-48	82.13	98.90	The column on the opposite side of the force	245	0.0144	144
			The column on the force side	525	0.0383	207
			The beam on the opposite side of the force	81	0.0155	157
RH-10-48-14	85.21	96.69	The column on the opposite side of the force	231	0.0136	130
			The column on the force side	495	0.0361	195
			The beam on the opposite side of the force	300	0.0175	163
RH-10-48-16	98.32	95.15	The column on the opposite side of the force	217	0.0128	122
			The middle of the beam span	280	0.0162	151
			The beam on the opposite side of the force	295	0.0175	162
RH-20-48-14	88.91	96.26	The column on the opposite side of the force	217	0.0121	120
			The middle of the beam span	287	0.0169	155
			The beam on the opposite side of the force	300	0.0178	163
RH-20-48-16	99.07	94.34	The column on the opposite side of the force	203	0.0116	110
			The middle of the beam span	287	0.0169	155
			The beam on the opposite side of the force	315	0.0190	170
RH-30-48-14	84.79	94.01	The column on the opposite side of the force	196	0.0112	106
			The middle of the beam span	301	0.0172	163
			The beam on the opposite side of the force	330	0.0210	180
RH-30-48-16	98.13	93.98	The column on the opposite side of the force	182	0.0101	97.3
			The middle of the beam span	301	0.0172	163

Based on the data of this table, with the increase in the reinforcement area in the columns of all frames, l_P and θ_P decrease in the columns and increase in the beam. The amount of change for beams and columns of reinforced concrete frames with 14 mm reinforcement is about 1.061 and 0.877 times, respectively compared to RC-10-48 frame. Also, it for beams and columns of frames with 16mm reinforcement is about 1.093 and 0.766 times respectively compared to RC-30-48 frame. l_P and θ_P of beams in reinforced composite HPFRCC frames with 14 mm reinforcement are 1.1-1.289 and 1.367-1.78 times RC-10-48 frame, respectively. While the values of these parameters in frames with 16 mm reinforcement are 1.22-1.3 and 1.52-1.83 times, respectively. In reinforced composite HPFRCC frames, the l_P and θ_P values of the columns are about 15% and 55% higher than the corresponding values in reinforced concrete frames, respectively.

The l_P and θ_P of beams in reinforced HPFRCC frames with 14 mm reinforcement are 1.23-1.33 and 1.53-1.88 times RC-30-48 frame, respectively. While the values of these parameters in frames with 16 mm reinforcement are 1.27-1.4 and 1.73-2.08 times, respectively. In reinforced HPFRCC frames, the l_P and θ_P values of the columns are about 28% and 84% higher than the corresponding values in reinforced concrete frames, respectively.

Conclusion

Based on the modeling done in this study by finite element numerical method and using ABAQUS software, the following results were obtained:

1- By increasing the vertical force on the frame, the yield corresponding lateral displacement in reinforced concrete, reinforced composite HPFRCC and HPFRCC frames decreased 13-41%, 24-41% and 17-34%, respectively.

2- With an increase in the vertical force on the frame, lateral bearing capacity in reinforced concrete, reinforced composite HPFRCC and HPFRCC frames decreased 1-2%, 1-4% and 2-7%, respectively.

3- Under different loading conditions, the ductility of the reinforced composite HPFRCC and HPFRCC frames increased by 5-77% and 1.48-2.25 times compared to the reinforced concrete frames, respectively.

4- Under different loading conditions, the tolerable lateral force for reinforced composite HPFRCC and HPFRCC frames increased by 3-17% and 5-20%, respectively, compared to reinforced concrete frames.

5- The amount of vertical load on the frame is effective in the formation process of plastic hinges in the frame. Also, the amount of plastic hinges in HPFRCC frames is much less than the damage observed in concrete and reinforced composite HPFRCC frames.

6- By increasing the compressive strength of concrete or HPFRCC frame, the curvature and length of the plastic hinge increases. In other words, the amount of curvature and length of the plastic hinge in the HPFRCC frames increases by about 22-30% and 2.06-2.43 times compared to the reinforced concrete frame, respectively. This increase in reinforced composite HPFRCC frames was about 6-18% and 64-87% compared to concrete frame.

7- By increasing the area of the reinforcements in the columns, the ultimate force on the frames increased, but their final displacement did not change much.

8- In reinforced concrete frames, by increasing the size of rebars from 12 to 14 mm and 16 mm, the force increased by 16% and 36%, respectively, and the lateral displacement decreased by 5.5% and 8%, respectively.

9- In reinforced composite HPFRCC frames, by increasing the size of the rebars from 12 to 14 mm and 16 mm, the force increased by 7% and 21%, respectively, and the lateral displacement decreased by 1.5% and 3%, respectively.

10- In HPFRCC frames, by increasing the size of rebars from 12 to 14 mm and 16 mm, the force increased by 5% and 20%, respectively, and the lateral displacement decreased by 3% and 4.5%, respectively.

11- By increasing the reinforcement area in the frame columns of all frames, the plastic hinge length (l_P) and the plastic hinge rotation (θ_P) decreased in the columns and increased in the beam.

References

[1] Abushawashi, N., & Vimonsatit, V. (2014). Use of Ferrocement Panel as Reinforced Concrete Slabs with Lightweight Blocks Infill. Second Australasia and Southeast Asian Conference, Bangkok, Thailand,

[2] Adhikari, S., & Patnaik, A. J. N. U. J. o. R. (2012). Potential applications of steel fibre reinforced concrete to improve seismic response of frame structures. 113.

[3] Billington, S. L., Lignos, D. G., Hanson, J. V., & Moreno-Luna, D. (2011). Response of high performance fiber reinforced concrete infill panels retrofitting steel moment-resisting frames. Proceedings, 8th International Conference in Urban Earthquake Engineering, Tokyo Institute of Technology,

[4] Dehghani, A., Nateghi-Alahi, F., & Fischer, G. J. E. S. (2015). Engineered cementitious composites for strengthening masonry infilled reinforced concrete frames. 105, 197-208.

[5] FUKUYAMA, H., TESHIGAWARA, M., SUWADA, H., & FUKUDA, A. (2004). HPFRCC DEVICE FOR SEISMIC RESPONSE CONTROL.

[6] Hemmati, A., Kheyroddin, A., Sharbatdar, M., Park, Y., Abolmaali, A. J. C., & Materials, B. (2016). Ductile behavior of high performance fiber reinforced cementitious composite (HPFRCC) frames. 115, 681-689.

[7] Jiří, Š., & Petr, D. (2015). Field tests of high performance fiber reinforced concrete slabs: Impact of contact and distant explosions. International Conference on Military Technologies (ICMT) 2015,

[8] Maya, L., & Albajar, L. (2012). Beam-column connections for precast concrete frames using high performance fiber reinforced cement composites. In High Performance Fiber Reinforced Cement Composites 6: HPFRCC 6 (pp. 347-354). Springer.

[9] Ozyildirim, H. C., & Vieira, M. (2008). Exploratory investigation of high-performance fiber-reinforced cementitious composites for crack control.

[10] Yao, S., Zhang, J. W., & Tu, Y. M. J. A. M. R. (2011). Discussion on HRBF500 Grain Reinforcement and C100 High-Performance Fiber Reinforced Cementitious Composites (HPFRCC) in the Civil Air Defense Work. 168, 1658-1664.